

Supplementary information

A. Numerical methods and setups

Our computational cell is one unit of the photonic crystal slab, and we imposed Bloch periodic boundary condition in the $x - y$ direction to determine the in-plane wavevector (k_x, k_y) . We put a broadband dipole source at a random position *inside the slab*, which excites resonances as well as BICs. By imposing perfectly matched layers (PMLs) boundaries in the z direction, any radiation from the slab is absorbed. After the dipole source has been turned off, we perform a harmonic inversion on the fields to obtain the resonance frequencies ($\omega_{\mathbf{k}}$) and their corresponding normalized radiative lifetime (Q_r). Q_r as a function of (k_x, k_y) is then plotted in Fig. 2a.

Following this numerical methods, the example mode profiles of the BICs are plotted in Fig. S1. In here, the z component of the electric field, E_z , is plotted for both types of BICs in Fig. 2a: the one at the center of the Brillouin zone (Fig. S1a) and the one off-center (Fig. S1b). Clearly both modes are spatially localized in the z direction and do not couple to radiation. Meanwhile, both modes are extended Bloch modes in the $x - y$ plane and therefore integrable within one unit cell, but not over the entire three-dimensional space.

B. Symmetry requirements for stable BICs

Here, we give the proof that stable BICs at arbitrary k points can be found when the system is invariant under $C_2^z T$ and σ_z operators, and that stable BICs at C_2^z -invariant k points can be found when the system has C_2^z symmetry. Here, C_2^z means 180° rotation around z axis, and T means the time reversal operator. The schematics of the symmetry requirement is summarized in Fig. S2.

In region I, systems are invariant under the symmetry operator $C_2^z T$, namely $\epsilon^*(x, y, z) = \epsilon(-x, -y, z)$. Let $\mathbf{u}_{\mathbf{k}}$ be an eigenfunction of the master operator²² $\Theta_{\mathbf{k}} = \frac{1}{\epsilon}(\nabla + i\mathbf{k}) \times (\nabla + i\mathbf{k}) \times$, and recall that \mathbf{k} here only has x and y components since we are considering a slab structure that does not have translational symmetry in z . A short derivation shows that at any \mathbf{k} point, $\mathbf{u}_{\mathbf{k}}(\mathbf{r})$ and $C_2^z \mathbf{u}_{\mathbf{k}}^*(C_2^z \mathbf{r})$ are both eigenfunctions of $\Theta_{\mathbf{k}}(\mathbf{r})$ with the same eigenvalue, so

they must differ at most by a phase factor,

$$\begin{aligned}\mathbf{u}_{\mathbf{k}}(\mathbf{r}) &= e^{i\theta_{\mathbf{k}}} C_2^z \mathbf{u}_{\mathbf{k}}^*(C_2^z \mathbf{r}) \\ &= e^{i\theta_{\mathbf{k}}} (-\mathbf{u}_{\mathbf{k}}^{x*}, -\mathbf{u}_{\mathbf{k}}^{y*}, \mathbf{u}_{\mathbf{k}}^{z*})|_{(-x, -y, z)}\end{aligned}\quad (\text{S.1})$$

Here $\theta_{\mathbf{k}}$ is an arbitrary phase factor. Meanwhile, we are free to multiply $\mathbf{u}_{\mathbf{k}}$ with any phase factor, and it remains a valid eigenfunction. For our purpose here, we explicitly choose the phase factor of $\mathbf{u}_{\mathbf{k}}$ such that $e^{i\theta_{\mathbf{k}}} = -1$ for all \mathbf{k} . With this choice, we can average over x and y to get $\mathbf{c}(\mathbf{k}) = \mathbf{c}^*(\mathbf{k})$ for all \mathbf{k} . That is, the polarization vector $\mathbf{c}(\mathbf{k})$ is purely real.

Using the fact that systems in region *I* also have the up-down mirror symmetry σ_z , namely $\epsilon(x, y, z) = \epsilon(x, y, -z)$, we can link the radiation loss above and below the photonic crystal slab denoted by \mathbf{c}^\uparrow and \mathbf{c}^\downarrow . At any \mathbf{k} point, $\mathbf{u}_{\mathbf{k}}(\mathbf{r})$ and $\sigma_z \mathbf{u}_{\mathbf{k}}(\sigma_z \mathbf{r})$ are both eigenfunctions of $\Theta_{\mathbf{k}}(\mathbf{r})$ with the same eigenvalue, so

$$\begin{aligned}\mathbf{u}_{\mathbf{k}}(\mathbf{r}) &= e^{i\psi_{\mathbf{k}}} \sigma_z \mathbf{u}_{\mathbf{k}}(\sigma_z \mathbf{r}) \\ &= e^{i\psi_{\mathbf{k}}} (\mathbf{u}_{\mathbf{k}}^x, \mathbf{u}_{\mathbf{k}}^y, -\mathbf{u}_{\mathbf{k}}^z)|_{(x, y, -z)}\end{aligned}\quad (\text{S.2})$$

with $\psi_{\mathbf{k}}$ being an arbitrary phase factor (not to be confused with the one in Eq. (S.1)). Since $\sigma_z^2 = 1$, we can apply Eq. (S.2) twice to show that $e^{i\psi_{\mathbf{k}}} = \pm 1$. Averaging over x and y , we see that $\mathbf{c}^\uparrow = \pm \mathbf{c}^\downarrow$.

After using these two symmetries, the number of independent real variables in all radiation coefficients $c_{x,y}^{\uparrow,\downarrow}$ has been reduced from 8 to 2. Given that the number of independent tuning parameters is also 2: (k_x, k_y) , we are able to get stable BICs. Note that the combination of $C_2^z T$ and σ_z is just one sufficient condition for stable BICs in photonic crystal slabs. There might be other different choices of symmetries. For example, PT and σ_z is equivalent to $C_2^z T$ and σ_z , where P is the inversion operator. Also, the requirement of σ_z is not necessary when there is leakage to one direction only (such as BICs on the surface of a photonic bandgap structure¹⁹).

In region *II*, stable BICs at C_2^z -invariant k points can be found. Systems in this region have C_2^z symmetry, namely $\epsilon(x, y, z) = \epsilon(-x, -y, z)$. k points are C_2^z -invariant when $-\mathbf{k} = \mathbf{k} + \mathbf{G}$, with \mathbf{G} being a reciprocal lattice vector. A short derivation shows that at any k point, $\mathbf{u}_{\mathbf{k}}(\mathbf{r})$ and $C_2^z \mathbf{u}_{-\mathbf{k}}(C_2^z \mathbf{r})$ are both eigenfunctions of $\Theta_{\mathbf{k}}(\mathbf{r})$ with the same eigenvalue, so

$$\mathbf{u}_{\mathbf{k}}(\mathbf{r}) = e^{i\gamma_{\mathbf{k}}} C_2^z \mathbf{u}_{-\mathbf{k}}(C_2^z \mathbf{r}), \quad (\text{S.3})$$

with $\gamma_{\mathbf{k}}$ being an arbitrary phase factor (not to be confused with the two phase factors above). At these high-symmetry \mathbf{k} points, using Bloch theorem we know: $\mathbf{u}_{-\mathbf{k}} = \mathbf{u}_{\mathbf{k}+\mathbf{G}} = \mathbf{u}_{\mathbf{k}}$, so we can apply Eq. (S.3) twice to get $e^{i\gamma_{\mathbf{k}}} = \pm 1$. When this factor is $+1$, we can average over x and y to see that $\mathbf{c}(\mathbf{k}) = 0$, corresponding to a BIC at this C_2^z -invariant k point.

In region III, both kinds of BICs can be found, where C_2^z , T and σ_z are all present. All our numerical examples are within this region to make it easier to understand the relation and interaction between different types of BICs.

C. Relationship between laser emission centered on BICs and vector beams

The far-field pattern at a definite \mathbf{k} point by itself does not reflect the vorticity of polarization around a BIC, but laser emission centered on such a BIC will. Laser emission always has a finite width in k -space and this wave-packet will be centered on the BIC; hence it will consist of a superposition of plane waves from the neighborhood of the BIC, leading naturally to a spatial twist in the polarization for the outgoing beam. Such beams have been studied previously, and are known as vector beams²¹, although their connection with BICs does not appear to have been realized. The number of twists in the polarization direction is known as the order number of the vector beam, and we now see that it is given by the topological charge carried by the BIC. Note that these vector beams are different from optical vortices, which usually have a fixed polarization direction.

D. Consequences of topological charge conservation

Since topological charge is a conserved quantity, there are a few consequences and restriction on the evolution of BICs. First, BICs are stable as long as the system retains required symmetries; however, perturbations that break these two required symmetries eliminate the existence of BICs. When C_2^zT symmetry is broken, the coefficients (c_x and c_y) require complex components, meaning the radiation becomes elliptically polarized instead of linearly polarized. When σ_z symmetry is broken, the coefficients $c_{x,y}^{\uparrow,\downarrow}$ are still real numbers, but radiation towards the top and towards the bottom become separate degrees of freedom and so they do not vanish simultaneously in general. Second, when BICs collide into each other in the moment space, the sum of all topological charges they carry remains the same before

and after the collision.

E. Example of charge -2

We consider the lowest-frequency TE-like mode of a photonic crystal slab with a hexagonal lattice of cylindrical air holes (shown in Fig. S4a). The refractive index of the slab is $n = 1.5$; the air-hole diameter is $0.5a$; and the thickness of the slab is $0.5a$, where a is the lattice constant. This system has C_6^z symmetry. Normalized lifetime plot indicates a BIC at the center of the Brillouin zone shown in Fig. S4b. The polarization vector field characterizes the BIC carrying charge -2 shown in Fig. S4c. Charge -2 can also be understood from the double degeneracy of both nodal lines of c_x (green) and c_y (red), shown in the inset of Fig. S4c. All four nodal lines are pinned at Γ point stabilized by the C_6 symmetry.

F. BICs related by point group symmetries have the same topological charges

Here, we prove that when the structure has a certain in-plane point group symmetry \mathcal{R} (namely, $\epsilon(\mathbf{r}) = \epsilon(\mathcal{R}\mathbf{r})$; \mathcal{R} can be a combination of rotation and reflection on the x - y plane) and when the band has no degeneracy, a BIC at \mathbf{k} indicates there is another BIC at $\mathcal{R}\mathbf{k}$ with the same topological charge. The assumption here is that the eigenfunctions $\mathbf{u}_\mathbf{k}$ at different k points already have their phases chosen to ensure the reality of $\mathbf{c}(\mathbf{k})$, and the signs of $\mathbf{u}_\mathbf{k}$ at different k points have been chosen such that $\mathbf{u}_\mathbf{k}$ is continuous with respect to \mathbf{k} (so that a small change in \mathbf{k} leads to a small change in $\mathbf{u}_\mathbf{k}$).

We start by relating the eigenfunction at \mathbf{k} and the eigenfunction at $\mathcal{R}\mathbf{k}$. Let $\mathbf{u}_\mathbf{k}$ be an eigenfunction of operator $\Theta_\mathbf{k}$. Since the system is invariant under transformation \mathcal{R} , we know $\hat{O}_\mathcal{R}\mathbf{u}_\mathbf{k}$ is an eigenfunction of $\Theta_{\mathcal{R}\mathbf{k}}$, so in the absence of degeneracy, we can write $\hat{O}_\mathcal{R}\mathbf{u}_\mathbf{k} = \alpha_\mathbf{k}\mathbf{u}_{\mathcal{R}\mathbf{k}}$, where $\alpha_\mathbf{k}$ is some number. The number $\alpha_\mathbf{k}$ must have unit magnitude (due to the normalization of $\mathbf{u}_\mathbf{k}$ and $\mathbf{u}_{\mathcal{R}\mathbf{k}}$) and must be real-valued (because $\mathbf{c}(\mathbf{k})$ is real-valued), so it can only take on discrete values of ± 1 . Also, $\alpha_\mathbf{k}$ must be a continuous function of \mathbf{k} since $\mathbf{u}_\mathbf{k}$ is continuous with respect to \mathbf{k} . Since $\alpha_\mathbf{k}$ is both discrete-valued and continuous, it must be a constant. Then, we may denote this constant with its value at the Γ point, as $\alpha_\mathbf{k} = \alpha_\Gamma$. Note that $\mathcal{R}\Gamma = \Gamma$, so we can determine coefficient α_Γ using the mode profile: $\hat{O}_\mathcal{R}\mathbf{u}_\Gamma = \alpha_\Gamma\mathbf{u}_\Gamma$. In conclusion, we have $\mathbf{u}_{\mathcal{R}\mathbf{k}} = \alpha_\Gamma\hat{O}_\mathcal{R}\mathbf{u}_\mathbf{k}$.

Now we consider how the angle $\phi(\mathcal{R}\mathbf{k})$ is related to $\phi(\mathbf{k})$. The vector field $\mathbf{u}_\mathbf{k}$ transforms under the rotation operator as $(\hat{O}_\mathcal{R}\mathbf{u}_\mathbf{k})(\mathbf{r}) = \mathcal{R}\mathbf{u}_\mathbf{k}(\mathcal{R}^{-1}\mathbf{r})$, so averaging over x and y we get $\langle \hat{O}_\mathcal{R}\mathbf{u}_\mathbf{k} \rangle = \mathcal{R}\langle \mathbf{u}_\mathbf{k} \rangle$. Let P be the operator that projects a 3D vector onto the x - y plane, namely $P\mathbf{r} = \mathbf{r} - (\mathbf{r} \cdot \hat{z})\hat{z}$; it commutes with \mathcal{R} , since it does not alter the x or y component. Then $\mathbf{c}(\mathbf{k}) = P\langle \mathbf{u}_\mathbf{k} \rangle$, and

$$\mathbf{c}(\mathcal{R}\mathbf{k}) = P\langle \mathbf{u}_{\mathcal{R}\mathbf{k}} \rangle = P\langle \alpha_\Gamma \hat{O}_\mathcal{R}\mathbf{u}_\mathbf{k} \rangle = \alpha_\Gamma \mathcal{R}P\langle \mathbf{u}_\mathbf{k} \rangle = \alpha_\Gamma \mathcal{R}\mathbf{c}(\mathbf{k}). \quad (\text{S.4})$$

So, the polarization vector at the transformed k point is simply the original polarization vector transformed and times ± 1 . So, the angle of the polarization vector only changes by a constant in the case of proper rotations (where $\det \mathcal{R} = 1$); in the case of improper rotations (where $\det \mathcal{R} = -1$), it also changes sign. So, in general, we can write

$$\phi(\mathcal{R}\mathbf{k}) = (\det \mathcal{R})\phi(\mathbf{k}) + c \quad (\text{S.5})$$

with c being a constant depending on \mathcal{R} and α_Γ . It follows that $\nabla_{\mathcal{R}\mathbf{k}}\phi(\mathcal{R}\mathbf{k}) = (\det \mathcal{R})\mathcal{R}\nabla_\mathbf{k}\phi(\mathbf{k})$, so the topological charge at $\mathcal{R}\mathbf{k}$ is

$$\begin{aligned} q_{\mathcal{R}\mathbf{k}} &= \frac{1}{2\pi} \oint_{C_{\mathcal{R}\mathbf{k}}} \nabla_{\mathbf{k}''} \phi(\mathbf{k}'') \cdot d\mathbf{k}'' \\ &= \frac{1}{2\pi} \oint_{\mathcal{R}^{-1}C_{\mathcal{R}\mathbf{k}}} \nabla_{\mathcal{R}\mathbf{k}'} \phi(\mathcal{R}\mathbf{k}') \cdot \mathcal{R}d\mathbf{k}' \\ &= \frac{1}{2\pi} (\det \mathcal{R}) \oint_{C_\mathbf{k}} \nabla_{\mathcal{R}\mathbf{k}'} \phi(\mathcal{R}\mathbf{k}') \cdot \mathcal{R}d\mathbf{k}' \\ &= \frac{1}{2\pi} (\det \mathcal{R})^2 \oint_{C_\mathbf{k}} \mathcal{R} \nabla_{\mathbf{k}'} \phi(\mathbf{k}') \cdot \mathcal{R}d\mathbf{k}' \\ &= q_\mathbf{k}, \end{aligned} \quad (\text{S.6})$$

where $C_{\mathcal{R}\mathbf{k}}$ is a closed simple path that is centered on $\mathcal{R}\mathbf{k}$ and loops in counterclockwise direction, $\mathcal{R}^{-1}C_{\mathcal{R}\mathbf{k}}$ is this loop transformed by \mathcal{R}^{-1} (which centers on \mathbf{k} in counterclockwise direction if \mathcal{R} is a proper rotation, or in clockwise direction if \mathcal{R} is improper), and $C_\mathbf{k}$ is this transformed loop traversed in counterclockwise direction.

In conclusion, we have proven that if a system has certain point group symmetry \mathcal{R} , then the topological charges carried by the BIC at \mathbf{k} and at $\mathcal{R}\mathbf{k}$ on a singly degenerate band have to be the same. This conclusion agrees with all examples in Figs. 2-3 and S3.

G. Allowed charges at Γ in systems with different symmetries

Allowed topological charges at high symmetry k points can be determined by the field eigenvalues of the rotational symmetry of a system. For systems with m -fold rotational symmetry, we can first determine the relationship between polarization direction at wavevector \mathbf{k} and at rotated wavevector $\mathcal{R}\mathbf{k}$ ($\phi(\mathbf{k})$ and $\phi(\mathcal{R}\mathbf{k})$) using Eq. (S.4). Since the wavevector gets back to its original point if applying this rotation m -times: $\mathcal{R}^m\mathbf{k} = \mathbf{k}$, we can then apply this relationship m times and get how many times the polarization vector rotates around the center of the Brillouin zone. From there, we categorize all possible charges allowed at Γ as shown in Table S1. Allowed charges depend on two factors. The first one is which symmetry representation the band belongs to. The second one is the degeneracy of nodal lines at Γ , because more nodal lines intersecting at the same point usually leads to more oscillations in color and thus higher topological charges. This factor is reflected by the integer number n , depending on the number of equivalent Γ points at this frequency⁴⁰. Note that only singly degenerate bands are considered in this Letter, having no crossing with other bands in the bandstructures, as can be seen in Table S1. Further research directions may include BICs on degenerate bands, as well as the search of BICs with higher-order and potentially fractional topological charges.

Symmetries	Representation	Charges	Allowed n	Allowed charges
C_2	A	$\pm 1 + 2n$	0	± 1
	B	$0 + 2n$		0
C_3	A	$1 + 3n$	$0, \pm 1, \dots$	$+1, +4, -2, \dots$
C_4	A	$1 + 4n$	$0, \pm 1, \dots$	$+1, +5, -3, \dots$
	B	$-1 + 4n$		$-1, -5, +3, \dots$
C_6	A	$1 + 6n$	$0, \pm 1, \dots$	$+1, +7, -5, \dots$
	B	$-2 + 6n$		$-2, +4, -8, \dots$

TABLE I. Allowed stable topological charges at Γ for singly degenerate bands. A(B) corresponds to modes of different representations of the symmetry operator⁴². Note that only singly degenerate representations of symmetry operators are included in here.

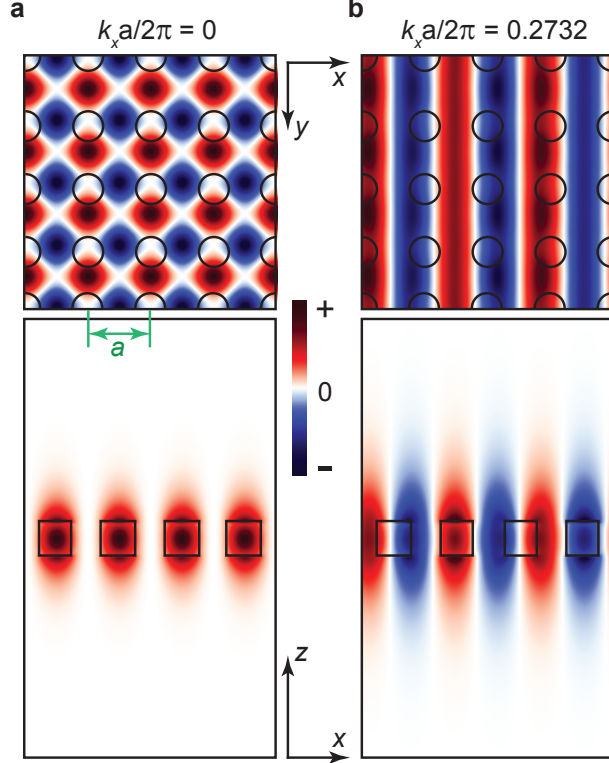


FIG. S1. Example mode profiles of BICs. **a**, The mode profiles of the z component of the electric field, \mathbf{E}_z , for the BIC at the center of the Brillouin zone shown in Fig. 2a. The upper part shows a slice of 4×4 unit cells on the $x-y$ plane at the center of the high index layer; while the lower part shows a slice on the $x-z$ plane. The color bar has with arbitrary units. **b**, The mode profiles of \mathbf{E}_z for the BIC on the positive k_x axis in Fig. 2a. Both modes are spatially localized in the z direction and do not couple to the radiation. Meanwhile, in the $x-y$ plane, they are both extended Bloch modes and are therefore integrable within one unit cell, but not over the entire three-dimensional space.

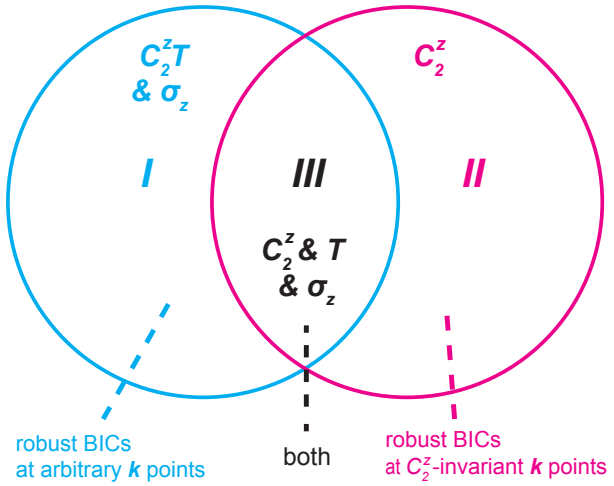


FIG. S2. Symmetry requirements for BICs. Systems in the blue circle are invariant under operators $C_2^z T$ and σ_z , where stable BICs at arbitrary wavevectors can be found. In the red circle, where C_2^z is a symmetry of the system, robust BICs can be found at high-symmetry wavevector points. Here, high-symmetry wavevectors mean C_2^z -invariant ones, while arbitrary wavevectors are not necessarily C_2^z -invariant. In the overlapping area (region *III*), both types BICs can be found. All numerical examples in this Letter are within region *III*.

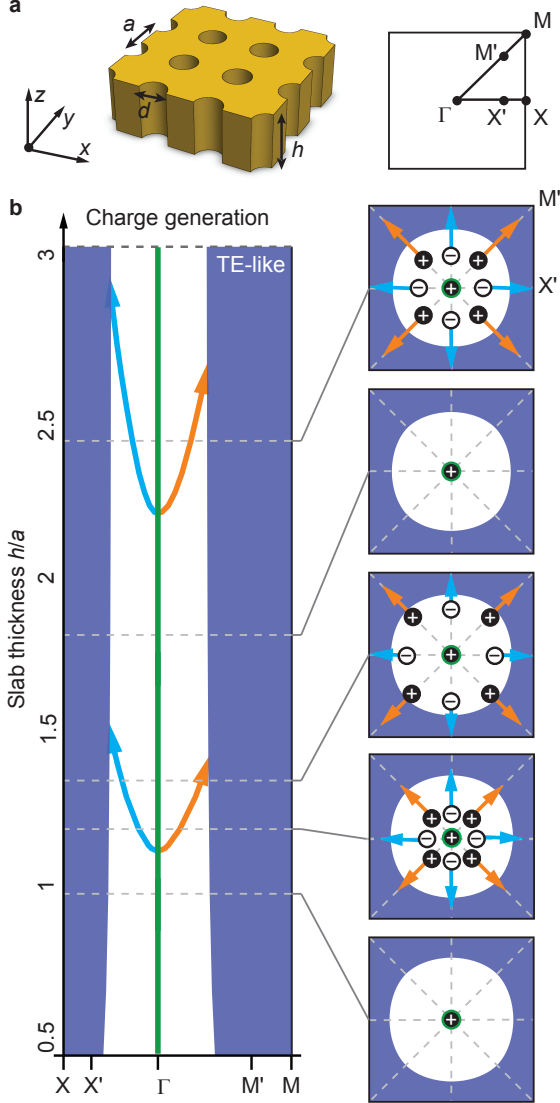


FIG. S3. Generation of BICs. **a**, Schematic drawing of a photonic crystal slab with two-dimensional periodicity. **b**, Generation of BICs on the TE_1 band when the slab thickness h is increased. Each time, four pairs of BICs with charges ± 1 are generated simultaneously, consistent with the charge conservation and C_{4v} symmetry. Insets show the locations of BICs in the k space and their corresponding topological charges for $h/a = 1.0, 1.2, 1.35, 1.8$, and 2.4 . As the slab thickness increases, the BICs move outward and eventually fall below the light line into the area shaded in dark blue.

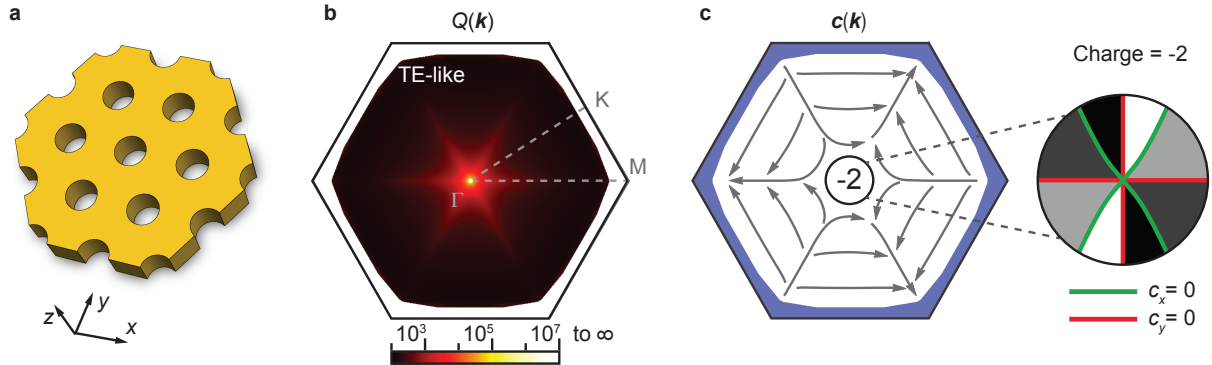


FIG. S4. Stable BIC with topological charge -2. **a**, Schematic drawing of the photonic crystal slab. **b**, Q plotted in the first Brillouin zone, showing a BIC at the Γ point. **c**, Polarization vector field characterizes the BIC with a stable topological charge of -2, as can be shown from double degeneracies of both nodal lines.